IEEE Access
Multidisciplinary | Rapid Review | Open Access Journal

Received October 18, 2018, accepted December 5, 2018, date of publication December 18, 2018,
date of current version January 11, 2019.

Digital Object Identifier 10.1109/ACCESS.2018.2888507

Multi-Channel System for Simultaneous *In Situ* Monitoring of Ion Flux and Membrane Potential in Plant Electrophysiology

ZI-YANG WANG[1,2], JIN-HAI LI[1,3], QIAO ZHOU[1,2], XIN-YU GAO[1,2], LI-FENG FAN[1,3], YONG-QIAN WANG[1,3], LIN XUE[4], ZHONG-YI WANG[1,2,3], AND LAN HUANG[1,3]

[1]College of Information and Electrical Engineering, China Agricultural University, Beijing 100083, China
[2]Key Laboratory of Agricultural Information Acquisition Technology, Ministry of Agriculture, Beijing 100083, China
[3]Key Laboratory of Modern Precision Agriculture System Integration Research, Ministry of Education, Beijing 100083, China
[4]Smart City College, Beijing Union University, Beijing 100101, China

Corresponding author: Lan Huang (hlan@cau.edu.cn)

This work was supported by the National Natural Science Foundation of China under Grant 61571443.

ABSTRACT Simultaneous detection of both ion flux and membrane potential *in vivo* and *in situ* in plants is a challenging research task. To explore the mechanisms of plant electrical activity, researchers urgently need to understand and determine the types of ions and the ion fluxes that pass in and out of cells during polarization and repolarization, but the required measurements are very difficult to perform. In this paper, we have developed a versatile system that can detect the ionic flux and the membrane potential, *in vivo* and *in situ*, simultaneously. The system uses a self-referencing ion-selective glass microelectrode and a membrane potential glass microelectrode as sensors. These sensors are linked through a preamplifier with high input impedance to a specific dynamic measurement system that can amplify small extracellular concentration gradient signals and realize simultaneous measurement of both the ion flux and the membrane potential. In addition, an interpolation fitting algorithm has been proposed to reduce the artifacts that are present in the *in situ* measurements during plant growth. The hydrogen ion fluxes in wheat roots were measured using the self-referencing ion-selective microelectrodes, and the proposed system was used to measure NaCl stimulation-induced changes in the membrane potentials and hydrogen ion fluxes of wheat root epidermal cells. The results demonstrate that the system can meet the ion flux and membrane potential measurement requirements.

INDEX TERMS Ion flux, membrane potential, microelectrode sensor, multi-channel recording system, plant electrical signal, weak signal detection.

I. INTRODUCTION

For more than a century, the exploration of plant electrophysiology has steadily improved as a result of progress in the development of a variety of applicable measurement techniques [1]. It is well known that the use of glass microelectrodes allows research to be conducted into plant electrophysiology on levels ranging from tissues and organs down to single cells, and even to single ion channels [2]–[5]. Various micropipette tip diameters and forms are used in the intracellular recording, voltage clamp, patch clamp, and extracellular ion flux recording techniques. In particular, the ion flux measurement technique has been popular in the plant electrophysiology field in recent years and it has also been used in a wide range of other applications, including food security, heavy metal detection, biology and medical science [6]–[13].

The development of these electrophysiological measurement techniques has made multi-source electrophysiological data available for use in studies that aim to discover the mechanisms responsible for electrical activity in plants. Voltage clamps and patch clamps are available for simultaneous *in vitro* measurements of the current and the membrane potential (MP). In 1979, Coster and Beilby proposed a modified Hodgkin-Huxley model of the action potential in *Chara* based on the voltage clamp technique [14]. Wang *et al.* [15] proposed an action potential model of a guard cell based on an analysis of patch clamp data published in a paper by other researchers. However, these models did not include the

electrophysiological data that can barely be recorded by the patch clamp and the voltage clamp, such as ion pump and transporter data. The currents produced by these transporters and ion pumps are too weak to be recorded using the patch clamp technique [16]. In addition, the patch clamp cannot capture transport processes if there is an electrically neutral state during ion transport, i.e., if the net current is equal to zero. In recent years, a series of models of plant activities have been proposed by Gradmann [17] and Sukhov *et al.* [18]. These models were not only reformulated on the basis of experimentally measured ion channel data but also in terms of some transporter parameters and ion concentration terms that help the models to simulate plant electrical activity more accurately. In addition, it may be possible to establish a new ion transport law using a complex multi-source data-driven mathematical model. Therefore, a multi-channel plant electrophysiological data recording system is required to acquire a variety of electrophysiological data effectively and simultaneously, including extracellular ion flux data, membrane potential data, and intracellular ion concentration data.

Both the membrane potential change and the ion flux parameters have apparent physiological significance in plants [19], [20]. When the root is stressed by the presence of salt, the amount of K^+ efflux can be associated with its salt tolerance [21], [22]. Additionally, salinity tolerance in halophytes is strongly related to the H^+ efflux caused by H^+-ATPase activity [23]. The ability to maintain the membrane potential is important for plant performance when waterlogged [24]. The membrane potential change that is induced by burning can gradually increase the flow of light energy that is absorbed, as observed previously in peas [25]. Current commercial ion flux measurement systems include the Self-referencing Ion Electrode Technique (SIET) with automated scanning system developed in the National Vibrating Probe Facility at Marine Biological Laboratory and the microelectrode ion flux estimation (MIFE) system developed by the University of Tasmania [26]–[30]. Low-noise amplifiers such as the FD223A or KS-750 (World Precision Instruments, 175 Sarasota Center Blvd. Sarasota, FL 34240) can be used to record membrane potentials or intracellular ion concentrations. Benet *et al.* [31] developed a single-channel system to record either the ion flux or the membrane potential in plants by selecting the different functions required in the system software. Notably, glass microelectrodes are used in all the techniques described above. The different measurement techniques require different tip shapes and fillings, which cause the resistance of the glass microelectrode to vary from several hundreds of MΩ to several GΩ. In addition, a wide detection range is required to measure the electrophysiological data of plants, given that the amplitude of the membrane potential is typically dozens of millivolts, while the amplitude of the ion flux data is only of the order of several microvolts. Therefore, specific weak signal detection techniques and noise reduction techniques must be developed for plant electrophysiological measurement instrumentation.

Importantly, while simultaneous monitoring of the ion flux and the membrane potential in a micrometer-scale space requires excellent experimental skills, the measurements can also be affected by the growth of the plant. Therefore, to enable acquisition of the two types of electrophysiological data for plant electrical activity while also overcoming the mutual interference that occurs during simultaneous recording and the difficulty of weak signal detection, a simultaneous measurement method is proposed in this paper, and a multi-channel prototype system is developed.

The rest of this paper is organized as follows. Section II illustrates the basic technique that is used in the proposed system and describes the design of every module and the associated software in detail. Section III presents the experimental results, evaluates the prototype system, and discusses the results obtained. Finally, in Section IV, conclusions are drawn and future work is outlined.

II. METHOD AND DESIGN

A. ION FLUX RECORDING TECHNIQUE

In 1990, Kühtreiber and Jaffe [32] originally obtained extracellular Ca^{2+} flux in a very small space based on Fick's law using a self-referencing ion selective electrode with a vibrating probe technique. Fig. 1 shows a diagram of the process used to record the ion flux and the membrane potential simultaneously. The ion selective glass microelectrode can detect the ion concentration gradients in a bath solution at a given distance ΔX, which represents the vibrating distance of the ion selective microelectrode between positions A and B. The electrical potentials of positions A and B are V_1 and V_2, respectively, and then the difference in concentration between the two positions (i.e., the difference in ion activity) can be calculated using V_1 and V_2. In practice, the Nernst slope of the ion selective microelectrode is determined via a calibration process; detailed descriptions of the process can be found in [27], [33], and [34]. In recordings of the membrane potential, the glass microelectrode is used to impale the cell, while the reference electrode is placed outside the cell. The resulting potential difference between these two electrodes represents the membrane potential.

In addition, glass microelectrodes are used to measure electrophysiological activity in plants. Glass microelectrodes with various tip diameters can be adapted to perform various measurements, including cell membrane potential and patch clamp measurements, plus ion flux detection [35]. Table 1 lists the main microelectrode sensors that are used in this system, including the glass microelectrodes for intracellular recording and the ion-selective glass microelectrodes. The glass microelectrode that is used for membrane potential detection requires a tip diameter of less than 1 μm for cell penetration. Unlike animal cells, plant cells usually have hard cell walls, so the neck of the glass microelectrode should not be either too long or too slender to enable penetration into the cytoplasm of the plant cells. The shape of the microelectrode

TABLE 1. Properties of the different microelectrodes.

Electrode	Tip diameters (μm)	Resistance (Ω)	Applications
Glass microelectrode	0.1-1	10^6-10^8	Cell impalement
Ion selective glass microelectrode	6-10	10^7-10^9	Specific ion flux and concentration recording

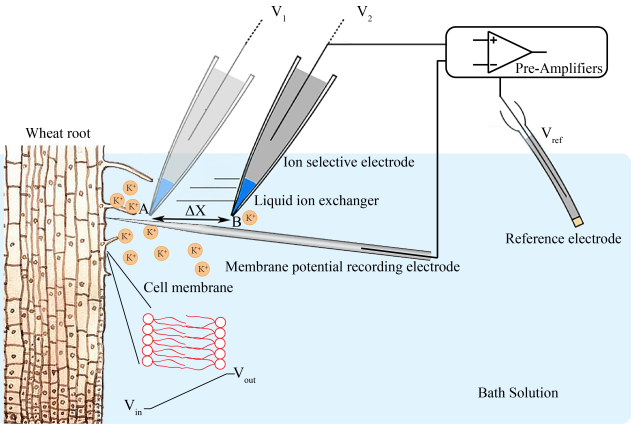

FIGURE 1. Schematic diagram of ion flux and membrane potential recording process.

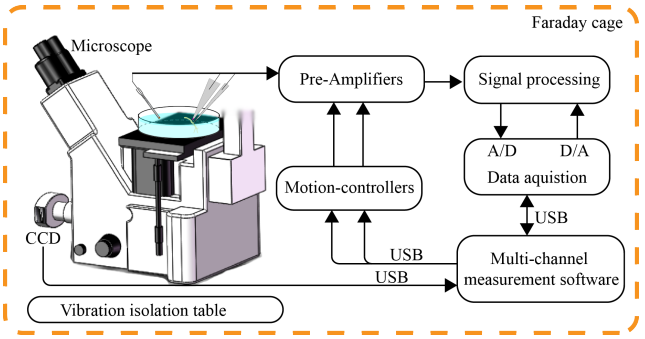

FIGURE 2. System diagram. Arrows indicate the directions of the signals and the commands. In the Faraday cage, commands are transmitted to the motorized manipulator via the USB interface from the multi-channel measurement software; these commands then control the motion of the pre-amplifier relative to the three-axis. The microelectrode is used to measure the ion flux and membrane potential data. Only one reference electrode is used in this system. The electrical signals are acquired using high-resistance preamplifiers and then pass through the signal conditioning circuit and enter the analog-to-digital board, which is connected to the multi-channel measurement software through the USB interface. The software offers the functions of a digital filter plus data display and storage. The software also connects to the CCD to record real-time images of samples and microelectrodes.

can be molded efficiently using capillary pullers controlling melting temperature and pull velocity and force. As shown in Fig. 1, the extracellular ion selective electrode consists of a glass microelectrode backfilled with electrolyte (liquid salt bridge) and tip filled with a liquid ion exchanger (LIX) contained in the tip of this electrode. The specific ion activity and the LIX junction potential follow a Nernstian manner [29].

B. SYSTEM DESIGN

A diagram of the system is shown in Fig. 2. The system can monitor extracellular ion flux and intracellular membrane potential in plants in real time. An inverted microscope (XDS-1B, Chongqing MIC Technology Co., Ltd, Chongqing, China) is used. Two high-precision three-axis motorized manipulators (CFT-8301D, Jiangsu Rich Life Science Instrument Co., Ltd, Jiangsu, China) are used to the control membrane potential recording electrode and the ion flux recording electrode. For the ion flux and membrane potential measurements, the glass microelectrode is mounted in a microelectrode holder that contains an Ag/AgCl wire, and a preamplifier with high input impedance is used to acquire and amplify the two required signals. These signals are then processed, passing through the low-pass filter and the differential amplifier in the conditioning circuits, before entering the 16-bit analog-to-digital board (USB-4716, Advantech Co., Ltd, Taiwan, China). The data acquisition module is controlled by the software through a Universal Serial Bus (USB) interface, and the software offers digital filtering, data display and data storage functions. The high-precision three-axis motorized manipulators are also controlled via the software. Images or videos of the plant sample are viewed in real time via the display of a charge coupled device (CCD) camera (TCC-4, Tucsen Imaging Technology Co., Ltd, Fuzhou, China) that is mounted on the microscope's side-port. The completed system is placed in a self-made Faraday cage, and the microscope is located on a vibration isolation table (AVT, Meiritz Seiki Co., Ltd, Japan).

1) PREAMPLIFIER

The microelectrode connection interface and the preamplifier were contained within a shielding box, which then allows simultaneous movement of the probe and preamplifier as a single unit. By reducing the length of the lead required, the reliability of the interface between the microelectrode and the preamplifier can be improved, and the noise of the head stage was also suppressed.

The electrical potential of the ion-selective microelectrode when filled with the LIX is the sum of all the interfacial local potentials, which will give a measurement range from the baseline to hundreds of millivolts. In addition, the membrane potential changes in plant cells in response to stimuli are often on the millivolt level. Therefore, to measure more types of plant electrophysiological data and adapt the system using more microelectrodes of different types, we designed a preamplifier to operate within an input range between −1000 mV and 1000 mV. As shown in Fig. 3, a preamplifier circuit was designed for the microelectrode with an input impedance of more than 10^{13} Ω, and this microelectrode could detect the voltage signal from a sensor effectively. Because of the differential amplification that occurred in the DC mode, the magnification of the preamplifier was set at

10× for the post-processing circuit of the signal processing circuit (see the circuit details below). The preamplifier is shielded using a small metal shell that is connected to the ground, and the output signal line was also shielded. Additionally, the ceramic insulation materials that were located at the interface of the holder were used to provide electrical isolation between the signal and ground.

2) SIGNAL PROCESSING CIRCUIT

It is important that the signal processing design takes the signal range into account while also ensuring that there is sufficient signal resolution in this multi-channel simultaneous recording system. In fact, it is very difficult to rely solely on the high-resolution analog-to-digital (A/D) converter. The signal range of the system ranged from −1000 mV to 1000 mV. If it is necessary to distinguish the signal changes at the 0.1 μV level, the bits of the A/D converter are calculated using the following formula:

$$\frac{\log_{10} \frac{2000\ mV}{0.1\ \mu V}}{\log_{10} 2} = 24.25 \text{ bit} \approx 24 \text{ bit} \tag{1}$$

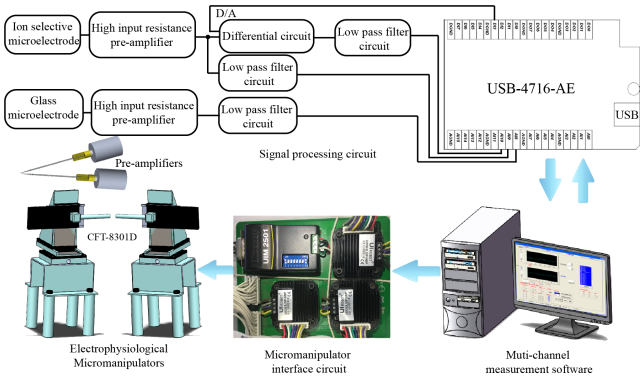

FIGURE 3. System circuit and interface diagram. The glass microelectrode and the preamplifier are connected using a yellow holder, the preamplifier is then connected to the filter and the differential amplifier circuit, while the other input of the differential amplifier is connected to the USB-4716 digital output terminal. The signals from the four channels pass through the low-pass filter and enter the analog-to-digital (A/D) data acquisition board for A/D conversion. The converted data are then transmitted to the software for further signal filtering and other processing. The software can be used to instruct the micromanipulator via the interface circuit.

Therefore, the system must use a 24-bit A/D converter. However, the noise level of the circuit is much higher than 0.1 μV, which means that is still difficult to distinguish 0.1 μV changes in the ion concentration gradients when using a 24-bit A/D converter. In this work, we used dynamic differential amplification technology to solve this problem. As shown in Fig. 1 and Fig. 3, when the electrode measures the signal V_1 at position A, it is then amplified 10 times by the preamplifier. After V_1 passes through a low-pass filter and is converted using the A/D converter, the digital quantity D_1 is given. D_1 is then sent to the digital-to-analog (D/A) converter, and VA_1 is the output value. Then, VA_1 is fed back to the differential amplifier's negative input, where the differential amplifier's magnification is 100×. Finally, the signal will pass through a low-pass filter with a cut-off frequency of 10 Hz. The output of the low-pass filter can then be calculated using:

$$dV_1 = (10 \times V_1 - VA_1) \times 100 \tag{2}$$

By holding VA_1 and moving the electrode to B, V_2 is then obtained and it is amplified 10 times by the preamplifier. The signal is then sent to the positive input of the differential amplifier. The output from the low-pass filter is calculated using:

$$dV_2 = (10 \times V_2 - VA_2) \times 100 \tag{3}$$

The dV that was obtained in this way is written as:

$$\mathrm{dV} = dV_2 - dV_1 = 1000 \times (V_2 - V_1) \tag{4}$$

$$\frac{\log_{10} \frac{2000\ mV}{0.1\ \mu V} \div 1000}{\log_{10} 2} = 14.29 \text{ bit} \approx 14 \text{ bit} \tag{5}$$

Therefore, the resolution required for the A/D converter is reduced by 1000 times by designing it in this way. Accordingly, a 16-bit A/D converter is used in this system, and can be implemented easily.

3) MOTORIZED MANIPULATOR

In this ion flux and membrane potential detection approach, the microelectrodes must be moved on the micrometer scale. Therefore, as shown in Table 2, we used a three-axis motorized manipulator with accuracy of 0.047 μm at a speed of 3 mm/s. The micro-integrated stepper motor control driver (UIM242, UI Robot Technology Co. Ltd, Shanghai, China) that controlled the three-axis motorized manipulator was controlled using the CAN2.0B standard with 1–16 step subdivision. Because we used a USB-serial port interface to send the instructions in the multi-channel measurement software, we also needed to control the protocol converter UIM2501 (UI Robot Technology Co. Ltd), which converted the CAN2.0B protocol to the RS232 protocol with a 115200 bps baud rate. The three-axis motorized manipulator and the interface converter module were powered using a 12 V 2 A DC supply.

TABLE 2. Technical parameters of the system.

Technical Parameters	Numerical Value
Number of channels	4
Accuracy of channel 1,2	0.3 μV
Accuracy of channel 3,4	305 μV
Drift	±30 μV/℃
pre-amplifier input range	±1 V
Travel	X=Y=Z=26 mm
Resolution	0.047 μm
Vertical rotation angle	360°
Horizontal rotation angle	120°

4) MULTI-CHANNEL MEASUREMENT SOFTWARE

We programmed the software in Microsoft Visual Basic running on Windows, and the functions of this software are shown in Fig. 4. Data that were acquired using the A/D board were transmitted to the software via the USB interface. Instructions were also sent by the software to control the three-axis motor controller via another USB interface. The software includes an initialization module, a data acquisition module, a data display module and a data storage module. The initialization module consists of data acquisition initialization and three-axis controller initialization processes. In this software, a module for two- or three-point calibration procedures, bracketing experimental ion concentrations, was programmed to calibrate the ion selective electrode before the ion flux recording experiment. This module can be used to confirm whether the ion selective electrode is available for each experiment. The software allows us to set the vibration parameters, including the vibrating distance (in μm), the holding time (s) and the vibrating direction selection (X, Y, and Z axes). Additionally, instructions can be sent directly to the motorized manipulator to control the movement of the preamplifier via the software.

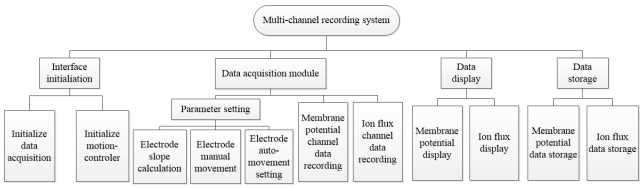

FIGURE 4. Functional diagram of the plant multi-channel electrophysiological data acquisition system.

A display window provides the functionality that allows curves to be drawn for the ion flux and membrane potential channels simultaneously in real time, which then enables observation of the simultaneous changes in the ion flux and the membrane potential in a simple manner. The ion flux data are stored in the comma-separated values filetype (csv) format in real-time, where the data include the current time, the value of the ion selective electrode, the electrical potential difference between the near- and far-pole positions of the ion selective electrode, and the relative position parameters of the X, Y, and Z axes. At the same time, the membrane potential data are also stored in csv format and include the current time and the membrane potential value. This multi-channel system can collect ion flux data with a frequency of 0.1–0.5 Hz and membrane potential data with a frequency of 10 Hz. Therefore, the two types of data can be stored in two different csv files simultaneously, which will allow researchers to analyze the data with strong correlations. Real-time video can also be collected via CCD displays using Tucsen Software (Tucsen Imaging Technology Co., Ltd, Fuzhou, China).

C. MATERIALS AND EXPERIMENTAL METHODS

1) PLANT MATERIALS

The wheat samples (5182) were obtained from the College of Agronomy and Biotechnology of China Agricultural University. The wheat seeds were disinfected using a 10% sodium hypochlorite solution for 15 min before germination and were then rinsed with deionized water three to six times. The wheat seeds were soaked (deionized water) in darkness for 12–24 h and were then grown on germination paper in Petri dishes. The deionized water and the germination paper were both replaced daily. The wheat samples were grown using a photoperiod of 14 (light)/10 (dark) h at 28/26 °C with relative humidity of 60% for 6–7 days.

2) FABRICATION OF THE GLASS MICROELECTRODE

Descriptions of the preparation of the membrane potential microelectrodes and the ion-selective microelectrodes have been given in detail in [29] and [36]. Briefly, for the membrane potential recording, glass micropipettes with filaments (B15024F, VitalSense Scientific Instruments Co., Ltd., Wuhan, China) were pulled using a micropipette puller (P-97, Sutter Instrument Co., Ltd., USA) with a tip diameter of $\sim$1 μm and a tip length of 6–12 mm. The membrane potential electrode can be used after being backfilled with 100 mM KCl and confirming that there are no insolating bubbles contained inside the electrode. Unlike the membrane potential electrode, the ion-selective microelectrodes are prepared using borosilicate glass capillaries without filaments (B15014N, VitalSense Scientific Instruments Co., Ltd.) to have a tip diameter of 6–10 μm and a tip length of 3–6 mm. In particular, the ion selective electrodes must be salinized [33]. These microelectrodes were backfilled with 100 mM KCl for K^+ ions and 15 mM NaCl plus 40 mM KH_2PO_4 (which was adjusted to a pH of 6.0 using NaOH) for H^+ ions. The microelectrode tips were then front-filled with ion selective K^+ (Potassium ionophore 1-cocktail A (60031), Linear range: 10^{-3} to 10^{-1} M KCl, Fluka, USA) and H^+ (Hydrogen ionophore 1-cocktail A (95291), pH linear range: 5.5 to 12, Fluka, USA) cocktails.

3) CALIBRATION OF THE ION SELECTIVE ELECTRODES

To achieve a high repeatability, ion selective electrode must be seriously prepared and calibrated before using. The relationship between the electrical potential E of the ion selective glass microelectrode and the ion concentration c around the tip of the electrode is given by (6).

$$\mathrm{E} = \mathrm{k} \pm \mathrm{s} \log c \tag{6}$$

where E has units of mV, and c is the concentration of the ions that are to be calibrated in the solution in mol/L; s is the Nernst slope in V/decade (dec); and k is the Nernst intercept (mV). The theoretical calculation of the Nernst slope s is given by (7):

$$\mathrm{s} = \frac{2.303RT}{nF} \tag{7}$$

where R is the gas constant (8.314 $JK^{-1} \cdot mol^{-1}$); T is the absolute temperature (K); F is the Faraday equivalent (9.6487.104 C mol^{-1}) and n is the ion charge number. The hydrogen ion selective electrode was calibrated using two

buffered solutions with pH values of 5.5 and 6.5 and the probe voltage was measured separately. The Nernst slope was calculated after the voltage stabilized. The theoretical slope for the hydrogen ion selective electrode is 59.16 mV/dec and the conversion efficiency of the ion selective electrode must be higher than 90% of the ideal slope (52 mV/dec) for it to be used [37].

Coefficient of variability (CV) was used to indicate the reliability for recording membrane potential and ion flux. $\mathrm{CV} \approx 1$ indicates a nearly random process; $CV \ll 1$ indicates a high stability. The calculation of the CV is given by: $\mathrm{CV} = |\sigma/\mu|$ where μ is the mean, and σ is the standard deviation.

III. RESULTS AND DISCUSSION

A. NOISE REDUCTION

Over the last two decades, while there have been some reports on the measurement of both ion flux and membrane potential, almost all the membrane potentials were sampled at intervals of several minutes [31], [38]. To investigate the mechanisms of the transmembrane ions, we developed a simultaneous measurement instrument to record the electrophysiological data of growing plants *in situ*. Unlike use of a high-pass filter, the differential amplifier in our system can amplify the difference between the D/A channel feedback voltage from the digital-to-analog conversion unit (16 bits D/A channel) and the bath solution potential to support a wide range of gradient measurements easily. This approach can not only obtain the ion flux but also can obtain the voltage of the ion-selective electrode, which reflects the ion activity of the bath solution at the recording position. In addition, to enable recording of multiple electrophysiological data simultaneously, more than two motorized manipulators can be manipulated simultaneously using the proposed system.

In reality, the sample always grows with a relatively fast speed for measurement *in situ*; for example, the maize root elongation rate is approximately 0.28–8.3 cm/day, while the root diameter also increases [39]. The growth of the sample may sometimes cause the electrode to move slowly out of the cell, and the recording membrane potential is then disturbed. When re-inserted into the cell, the electrical potential drops again. However, the raw curve must be corrected to recover the real signal. Recording of the plant membrane potential *in situ* is a highly difficult technique-dependent operation that always requires high-level experimental skills. To overcome the problems that are caused by continuous sample growth during simultaneous recording of the ion flux and the membrane potential, an interpolation algorithm was used in this work. In addition, the system's noise removal design is also a significant factor. In the plant electrophysiology field, the recorded signals are always accompanied by noise and drift problems, including power frequency noise, the thermal noise of the electrodes, the $1/f$ noise of the circuit system and environmental noise, which is mainly caused by human manipulation. The power frequency interference is primarily at 50 Hz (China), which will be coupled into the electrode circuit. Therefore, as the internal resistance of the microelectrode increases, it becomes increasingly susceptible to electronic interference. The thermal noise of the electrode and the $1/f$ noise of the soldered junction are difficult-to-avoid noise sources that both affect the ion flux data.

To remove any unwanted noise and drift, several methods for shielding from electromagnetic interference were applied in our system. A Faraday cage made from copper mesh was used to wrap the system and was connected to the ground. All the subsystems shown in Fig. 2 were shielded using a Faraday cage, which was grounded using a single-point grounding technique. Both the pre-amplifier and the signal processing circuit were powered using a lithium-ion battery in parallel with two bypass capacitors, including a 1 μF tantalum capacitor and a 22 pF ceramic capacitor. The analog low-pass filters and the digital filtering algorithms helped to reduce the system noise. We used a passive low-pass filter with a cutoff frequency of 10 Hz to acquire the membrane potential data. A first-order active low-pass filter, again with a cutoff frequency of 10 Hz, was used to remove the power and other environmental noise from the ion flux acquisition channels. To remove the power line interference (at 50 Hz in China), sampling times that were multiples of the fundamental power cycle were adopted, e.g., 60 ms, and the voltage data obtained were averaged. As a result, the system noise amplitudes of the ion flux acquisition channels and the membrane potential acquisition channel were less than 3 μV and 20 μV, respectively.

The system noise was evaluated using the standard deviation value obtained by shorting the input and measuring in the bath without a sample being present. Six samples were recorded (with 16 data points per sample), and the standard deviations were calculated for these 16 points for each sample before the averages and the standard deviations of those samples were calculated, with results as shown in Table 3. Because there was drift in both the membrane potential electrode and the ion flux electrode in the solution, when more data points are acquired over a longer time, the calculated standard deviations would be primarily influenced by the independent drift rather than the noise. Therefore, we only used 16 data points for the noise evaluation. For investigation of the noise level of the membrane potential recording channel, the time required to acquire 16 data points was less than 2 s, while the 16 data points were collected via the ion flux channel at a sampling rate of 0.3 Hz in 48 s. In this short recording time period, we considered the effects of the drift to be negligible. As shown in Table 3, when the shorted input of the pre-amplifier was connected to the membrane potential recording channel, the recorded voltage fluctuation was less than 20 μV. When the MP recording electrode (tip diameter of less than 1μm) and the reference electrode were immersed in the bath solution (1 mM KCl, 0.1 mM $CaCl_2$, with pH of 6.0), the voltage fluctuations increased slightly. Because the amplitude of the membrane potential ranges from several millivolts to hundreds of millivolts, this noise

TABLE 3. Noise from short input and solution.

Channel	Value
Shorted input of MP channel	0.013±0.002 mV
Shorted input of V1 of ion flux channel	0.14±0.07 mV
Shorted input of ΔV of ion flux channel	1.7±0.7 μV
Experimental noise of MP channel	0.02±0.01 mV
Experimental noise of V1 of ion flux channel	0.19±0.09 mV
Experimental noise of ΔV of ion flux channel	6.1±1.7 μV

has little effect on the acquired data. The V_1 value of the ion flux channel represents the ion concentration near the electrode tip in millivolts, while the ΔV value can be used to calculate the ion flux in microvolts. Using hydrogen as an example, the standard deviation of the ΔV value of the ion flux channel in the solution is approximately 4–10 μV, and the calculated flux is approximately 0.2–0.9 pmol $cm^{-2} \cdot s^{-1}$. This level of variation is acceptable in these measurements.

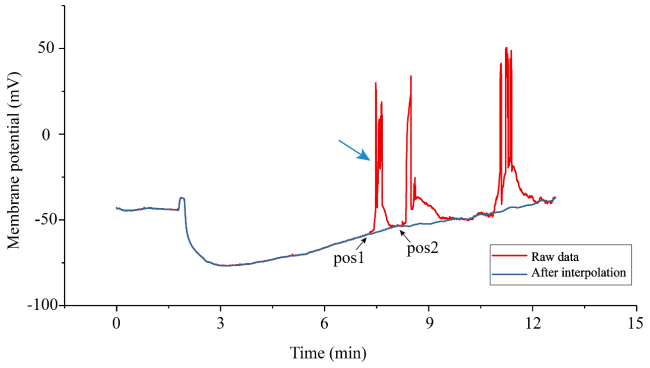

FIGURE 5. Schematic diagram of the interpolation algorithm. The figure shows the membrane potential data that recorded by the microelectrode inserted into the cells. The interference occurred in red line caused by the withdrawn microelectrode. The blue arrow indicates the interference to be eliminated, while the black arrows indicate Position 1 and Position 2, as used by the interpolation algorithm.

To reduce the known artifacts, noise and interference due to sample growth, an interpolation fitting algorithm has been proposed in this work. The interpolation algorithm was performed in the software. The results obtained when a microelectrode was taken out of the cell and then re-inserted into the cell are shown in Fig. 5. When a sudden voltage fluctuation occurs at random, the microelectrode may have moved to outside the cell. If the microelectrode is adjusted to impale the cell again in time, the experimental results apparently could not be influenced. The resulting suddenly rising curve could be removed using an interpolation fitting approach.

The interpolation algorithm is described in (8). Here, n is the sampling length at time of fitting, and generally constitutes 1/20 of the signal length. L is the span threshold that was set in the fitting, which generally has a value that is less than n. When the distance between peaks pos1 and pos2 (as indicated by the black arrow in Fig. 5) is greater than L, the slope k is determined by the values of pos1 and pos2; otherwise k is determined by the distance n before pos1.

$$y_i = \begin{cases} k\left(x_i - x_{(i-n)}\right) + y_{(i-n)}, & pos2 - pos1 > L \\ k\left(x_i - x_{(i-pos1)}\right) + y_{(i-pos1)}, & pos2 - pos1 \le L \end{cases}, \quad i \in [pos1, pos2] \tag{8}$$

B. ARTIFICIAL ION POINT SOURCE EXPERIMENT

An artificial ion source is generally used to determine the frequency dependence and the sensitivity of the vibrating ion selective microelectrode (for further details of the fabrication of an artificial ion source, the reader is referred to [32] and [34]). In this paper, an artificial K^+ source with a tip diameter of 40–50 μm that was filled with 200 mM KCl plus 0.5% agar was fabricated. The Nernst slope of this test electrode in the experiments was 53.27 mV/dec. In the experiments, two glass slides were placed tightly together at the bottom of a Petri dish (9 cm in diameter). The artificial K^+ source pipette was then taped onto the slide and the tip adjusted to have the same focal plane as the microscope. A bath solution (1 mM KCl, 0.1 mM CaCl2, with pH of 6.0) was added to the Petri dish. The prepared ion selective electrode was then adjusted to have the same focal plane as the microscope, as shown in Fig. 6(a). The ion-selective electrode vibrated at a frequency of 0.5 Hz within a distance of 30 μm along the X-axis, which was nearly 80 μm away from the source. The red curve plotted in Fig. 6(b) shows the raw data for the vibrating probe at each position. The data show the same "square wave oscillation" that was reported in [27] and [29]. The blue line depicting ΔV is the differential voltage obtained by comparing the average voltages at the two positions and this ΔV value can be converted into a flux value. The experiment indicates that the system can record the potential change in the ion-selective microelectrode over a short vibrating distance effectively, and the differential between the extremes of the vibration remains stable. Comparing with the fluctuation of ΔV value in Table 3, this stable acquired data shown in Fig. 6 proved that the system is reliable in ion flux recording.

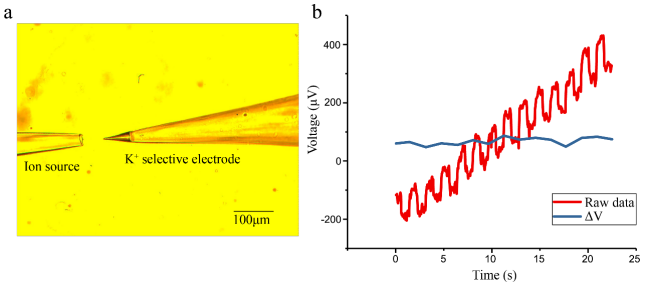

FIGURE 6. Ion source experiment. (a) Photograph of the K^+ source and the potassium ion selective electrode. (b) The red curve shows the original value of the electrode vibration during recording of the K^+ flux. The blue curve represents the differential value between the extremes of the vibration.

C. MEMBRANE POTENTIAL RECORDING EXPERIMENT

An *in situ* epidermal cell membrane potential measurement of the wheat root experiment was performed as an example of the potential application of our system. The depolarization and repolarization of the membrane potential have been monitored under NaCl stimulation. In the experiment, we prepared a pipette with a tip diameter of more than 100 μm to act as the stimulation electrode (filled with 2 M NaCl). First, the root samples were immobilized on a glass slide in a Petri dish, and then, the bath solution was used to fill the Petri dish. Second, the wheat root was moved to the focal plane of the microscope, and the stimulation electrode was moved slightly to have the same focal plane as the microscope using a three-axis motorized manipulator. The stimulation pipette was then raised out of the solution via the Z-axis. After the membrane potential electrode pierced the wheat root zone epidermal cells, the tip of the stimulation pipette was moved slowly near the membrane potential recording area, as shown in Fig. 7(a) and (b). The membrane potential data are shown in Fig. 7(c). When the stimulation pipette approached the membrane potential recording area, the epidermal cells were depolarized because of the diffusion of the high-concentration salt solution from the stimulation pipette. When the stimulating pipette was moved away from the wheat root, the concentration of the NaCl diffusion was then reduced and the epidermal cell membrane potential was repolarized, as indicated by the arrows shown in Fig. 7(c). The electrical potential value was not return to the pre-impalement level maybe caused by the tip obstruction, which changed the tip potential of the microelectrode. This NaCl-induced depolarization phenomenon is similar to that observed in the membrane potential studies of *Arabidopsis thaliana* roots (50 mM NaCl induced 60 mV depolarization) and possible ion mechanism in barley roots that were performed using the existing salt stimulation [36], [40]. This indicates that the system can record changes in the plant cell's membrane potential. The CV values in recording resting membrane potential in wheat root were in the range of 0.2%-0.6% ($n = 4$), which indicated that the system has a high reliability on recording membrane potential.

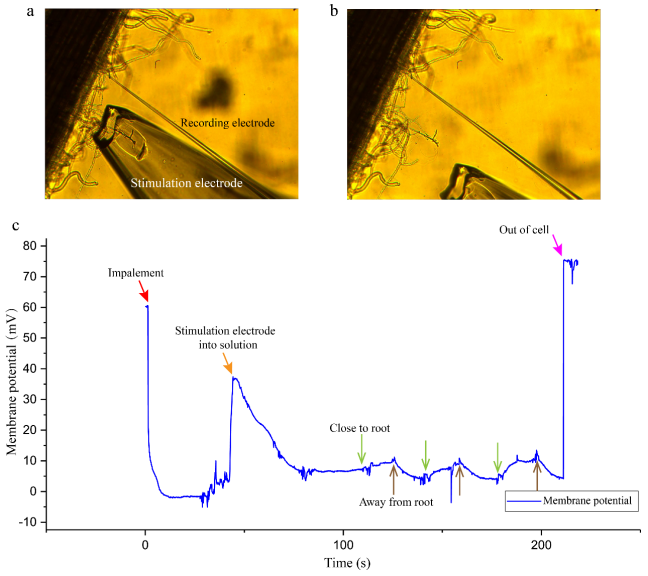

FIGURE 7. Membrane potential recording of the root epidermal cell in wheat. (a) The stimulation pipette is located close to the membrane potential recording area of the wheat root. (b) The stimulation pipette is taken away from the membrane potential recording area. (c) Membrane potential data, where the red arrow indicates the impalement and the orange arrow indicates the effect of the stimulation pipette moving into the solution. After the baseline stabilized, the green arrow indicates where the stimulation pipette was close to the membrane potential recording area, and the brown arrow shows when the stimulation pipette was moved away from the membrane potential recording area. The purple arrow indicates where the membrane potential electrode moved out of the wheat root epidermal cells.

D. SIMULTANEOUS H^+ FLUX AND MEMBRANE POTENTIAL RECORDING

The system can monitor both the membrane potential and the extracellular ion flux *in situ* simultaneously. In this example, simultaneous recording of the H^+ flux and the membrane potential in the wheat root was performed *in situ*. First, two motorized manipulators were used to move the tips of the membrane potential recording microelectrode and the H^+ selective microelectrode to one side of the sample. Because recording of the membrane potential always requires high experimental skill and may fail during impalement of the sample, we always impaled the cell at a suitable position before moving the ion-selective microelectrode near the cell to be measured. After the epidermal cell was impaled, the H^+ selective microelectrode was moved to a distance of 10–20 μm from the measurement area to monitor the H^+ flux, as shown in Fig. 8(a). Next, the added salt solution was taken away from the experimental region when the membrane potential was completely stable. We used 38 mL of the bath solution (1 mM KCl, 0.1 mM $CaCl_2$, with pH of 6.0), and 2 mL of 3 M NaCl was used as the salt stimulation solution. The NaCl concentration would be close to 150 mM after diffusion of the stimulating solution.

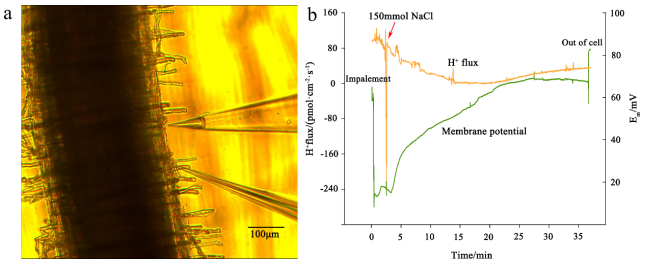

FIGURE 8. Simultaneous measurement of the H^+ flux and the membrane potential in the epidermal cell of the wheat root. (a) Photograph of the membrane potential and H^+ flux being recorded simultaneously. (b) H^+ flux and epidermal cell membrane potential data. The green curve is the epidermal cell membrane potential, while the orange curve is the H^+ flux (efflux positive). The red arrow indicates 150 mM NaCl stimulation.

Fig. 8b illustrates the results obtained from simultaneous monitoring of the epidermal cell membrane potential in the

wheat root and the extracellular H^+ flux. The result suggests that there was no interference exists between the contiguous measuring microelectrodes. The H^+ flux had an obviously decreasing efflux after the salt stimulation, with even a small influx, while the epidermal cell membrane potential depolarized simultaneously. The values of the H^+ flux and the membrane potential changed to have the opposite direction after salt stimulation for 20 min. The membrane potential tended to become stable and gradually repolarized, while the H^+ flux began to recover to the efflux stage. Because they were recorded simultaneously, the real-time correlation between epidermal cell membrane potential and H^+ flux can be obtained easily. The reduction in the efflux of H^+ and the depolarization of the cell membrane potential may reflect the hydrogen transmembrane mechanism. The H^+ efflux may support the depolarization of the epidermal cell, which is consistent with the results reported by other research groups [41]. The results demonstrated that the system can reliably and simultaneously monitor the ion flux and membrane potential in plant roots for above 30 mins. The CV values in recording H^+ flux in wheat root were in the range of 0.1%-4% ($n = 5$), which indicated that the system has a high reliability on recording ion flux.

IV. CONCLUSIONS

The multi-channel recording system for plant electrophysiology described here can monitor the ion flux and trans-membrane potential simultaneously in a growing plant. In this paper, three experiments were performed to evaluate the system's reliability, including the artificial ion source experiment, *in situ* measurements of the membrane potential, and simultaneous monitoring of the H^+ ion flux and the membrane potential of an epidermal cell in a wheat root. The results demonstrate that this system can acquire weak extracellular ion flux signals with high precision and can effectively remove the effects of sharp changes caused by plant growth or environmental change. Our system allows researchers to acquire, compare and analyze different types of plant electrophysiological data. In future explorations, this system will enrich the existing data and supply new data for plant electrical activity modeling. Furthermore, this system can also improve the efficiency of plant electrophysiological data measurements while reducing the experimental period required. This system will enrich bioelectronics research, expand the potential application range of the sensor technology, and provide innovative scientific tools that will allow researchers to study the mechanisms of plants and their environmental correlations.

REFERENCES

[1] R. Hedrich, V. Salvador-Recatalà, and I. Dreyer, "Electrical wiring and long-distance plant communication," *Trends Plant Sci.*, vol. 21, no. 5, pp. 376–387, May 2016.
[2] H. H. Dixon, "Transmission of stimuli in plants," *Nature*, vol. 114, p. 626, Jan./Jun. 1925.
[3] D. Gradmann and F. W. Bentrup, "Light-induced membrane potential changes and rectification in *Acetabularia*," *Naturwissenschaften*, vol. 57, no. 1, pp. 46–47, 1970.
[4] B. G. Pickard, "Action potentials resulting from mechanical stimulation of pea epicotyls," *Planta*, vol. 97, no. 2, pp. 106–115, 1971.
[5] R. Hedrich, "Ion channels in plants," *Physiol. Rev.*, vol. 92, no. 4, pp. 1777–1811, Oct. 2012.
[6] Z. Shen *et al.*, "Populus euphratica HSF binds the promoter of *WRKY1* to enhance salt tolerance," *Plant Sci.*, vol. 235, pp. 89–100, Jun. 2015.
[7] Y. Yang *et al.*, "Overexpression of the *PtSOS2* gene improves tolerance to salt stress in transgenic poplar plants," *Plant Biotechnol. J.*, vol. 13, no. 7, pp. 962–973, Sep. 2015.
[8] H. Wang, L. Shabala, M. Zhou, and S. Shabala, "Hydrogen peroxide-induced root Ca^{2+} and K^+ fluxes correlate with salt tolerance in cereals: Towards the cell-based phenotyping," *Int. J. Mol. Sci.*, vol. 19, no. 3, p. 702, Mar. 2018.
[9] T. M. Kang, V. S. Markin, and D. W. Hilgemann, "Ion fluxes in giant excised cardiac membrane patches detected and quantified with ion-selective microelectrodes," *J. Gen. Physiol.*, vol. 121, no. 4, pp. 325–347, Apr. 2003.
[10] L. Q. Cheng, M. W. House, W. J. Weiss, and M. K. Banks, "Monitoring sulfide-oxidizing biofilm activity on cement surfaces using non-invasive self-referencing microsensors," *Water Res.*, vol. 89, pp. 321–329, Feb. 2016.
[11] E. S. McLamore, M. C. Stensberg, M. S. Sepúlveda, W. Zhang, M. K. Banks, and D. M. Porterfield, "A self-referencing microelectrode for real time measurements of silver flux," *Sens. Actuators B, Chem.*, vol. 153, no. 2, pp. 445–452, Apr. 2011.
[12] E. S. McLamore *et al.*, "A self referencing platinum nanoparticle decorated enzyme-based microbiosensor for real time measurement of physiological glucose transport," *Biosensors Bioelectron.*, vol. 26, no. 5, pp. 2237–2245, Jan. 2011.
[13] B. C. Sanchez, H. Ochoa-Acuña, D. M. Porterfield, and M. S. Sepúlveda, "Oxygen flux as an indicator of physiological stress in fathead minnow *(Pimephales promelas)* embryos: A real-time biomonitoring system of water quality," *Environ. Sci. Technol.*, vol. 42, no. 18, pp. 7010–7017, Sep. 2008.
[14] M. J. Beilby and H. G. L. Coster, "The action potential in *Chara corallina* III.* The Hodgkin–Huxley parameters for the plasmalemma," *Austral. J. Plant Physiol.*, vol. 6, no. 3, pp. 337–353, 1979.
[15] Z. Wang *et al.*, "A theory model for description of the electrical signals in plant part—I," in *Proc. IFIP TC 12th Int. Conf. Comput. Comput. Technol. Agricult.*, 2007, pp. 637–643.
[16] Y. Nakanishi, I. Yabe, and M. Maeshima, "Patch clamp analysis of a H^+ pump heterologously expressed in giant yeast vacuoles," *J. Biochem.*, vol. 134, no. 4, pp. 615–623, Oct. 2003.
[17] D. Gradmann, "Models for oscillations in plants," *Austral. J. Plant Physiol.*, vol. 28, no. 7, pp. 577–590, 2001.
[18] E. Sukhova, E. Akinchits, and V. Sukhov, "Mathematical models of electrical activity in plants," *J. Membrane Biol.*, vol. 250, no. 5, pp. 407–423, Oct. 2017.
[19] V. Demidchik, S. Shabala, S. Isayenkov, T. A. Cuin, and I. Pottosin, "Calcium transport across plant membranes: Mechanisms and functions," *New Phytol.*, vol. 220, no. 1, pp. 49–69, Oct. 2018.
[20] R. Hedrich, "Ion channels in plants," *Physiol. Rev.*, vol. 92, no. 4, pp. 1777–1811, Oct. 2012.
[21] S. Shabala, "Signalling by potassium: Another second messenger to add to the list?" *J. Experim. Botany*, vol. 68, no. 15, pp. 4003–4007, Jul. 2017.
[22] F. Wang *et al.*, "Revealing the roles of GORK channels and NADPH oxidase in acclimation to hypoxia in *Arabidopsis*," *J. Experim. Botany*, vol. 68, no. 12, pp. 3191–3204, Jun. 2017.
[23] J. Bose, A. Rodrigo-Moreno, D. W. Lai, Y. J. Xie, W. B. Shen, and S. Shabala, "Rapid regulation of the plasma membrane H^+-ATPase activity is essential to salinity tolerance in two halophyte species, Atriplex lentiformis and Chenopodium quinoa," *Ann. Botany*, vol. 115, no. 3, pp. 481–494, Feb. 2015.
[24] F. R. Zeng *et al.*, "Linking oxygen availability with membrane potential maintenance and K^+ retention of barley roots: Implications for waterlogging stress tolerance," *Plant Cell Environ.*, vol. 37, no. 10, pp. 2325–2338, Oct. 2014.
[25] E. Sukhova, M. Mudrilov, V. Vodeneev, and V. Sukhov, "Influence of the variation potential on photosynthetic flows of light energy and electrons in pea," *Photosynthesis Res.*, vol. 136, no. 2, pp. 215–228, May 2018.
[26] C. Pandolfi, S. Mugnai, E. Azzarello, E. Masi, S. Pollastri, and S. Mancuso, "The vibrating probe technique in the study of root physiology under stress," in *Measuring Roots: An Updated Approach*. Berlin, Germany: Springer, 2012, pp. 67–81.

[27] I. A. Newman, "Ion transport in roots: Measurement of fluxes using ion-selective microelectrodes to characterize transporter function," *Plant Cell Environ.*, vol. 24, no. 1, pp. 1–14, Jan. 2001.
[28] H. H. Felle and P. K. Hepler, "The cytosolic Ca^{2+} concentration gradient of Sinapis alba root hairs as revealed by Ca^{2+}-selective microelectrode tests and fura-dextran ratio imaging," *Plant Physiol.*, vol. 114, no. 1, pp. 39–45, May 1997.
[29] P. J. S. Smith, K. Hammar, D. M. Porterfield, R. H. Sanger, and J. R. Trimarchi, "Self-referencing, non-invasive, ion selective electrode for single cell detection of trans-plasma membrane calcium flux," *Microsc. Res. Techn.*, vol. 46, no. 6, pp. 398–417, Sep. 1999.
[30] L. V. Kochian, J. E. Shaff, W. M. Kühtreiber, L. F. Jaffe, and W. J. Lucas, "Use of an extracellular, ion-selective, vibrating microelectrode system for the quantification of K^+, H^+, and Ca^{2+} fluxes in maize roots and maize suspension cells," *Planta*, vol. 188, no. 4, pp. 601–610, Nov./Dec. 1992.
[31] G. Gunsé, C. Poschenrieder, S. Rankl, P. Schröeder, A. Rodrigo-Moreno, and J. Barceló, "A highly versatile and easily configurable system for plant electrophysiology," *Methodsx*, vol. 3, pp. 436–451, May 2016.
[32] W. M. Kühtreiber and L. F. Jaffe, "Detection of extracellular calcium gradients with a calcium-specific vibrating electrode," *J. Cell Biol.*, vol. 110, no. 5, pp. 1565–1573, May 1990.
[33] L. Xue *et al.*, "The calibration model in potassium ion flux non-invasive measurement of plants *in vivo in situ*," *Inf. Process. Agricult.*, vol. 3, no. 2, pp. 76–82, 2016.
[34] P. J. S. Smith, R. H. Sanger, and L. F. Jaffe, "The vibrating Ca^{2+} electrode: A new technique for detecting plasma-membrane regions of Ca^{2+} influx and efflux," *Methods Cell Biol.*, vol. 40, vol. 40, pp. 115–134, 1994.
[35] X. Yan *et al.*, "Research progress on electrical signals in higher plants," *Progr. Natural Sci.*, vol. 19, no. 5, pp. 531–541, May 2009.
[36] L. Shabala, T. A. Cuin, I. A. Newman, and S. Shabala, "Salinity-induced ion flux patterns from the excised roots of *Arabidopsis* sos mutants," *Planta*, vol. 222, no. 6, pp. 1041–1050, Dec. 2005.
[37] *Chemical Sensors Research Group*. [Online]. Available: http://csrg.ch.pw.edu.pl/glossary/
[38] S. N. Shabala, I. A. Newman, and J. Morris, "Oscillations in H^+ and Ca^{2+} ion fluxes around the elongation region of corn roots and effects of external pH," *Plant Physiol.*, vol. 113, no. 1, pp. 111–118, Jan. 1997.
[39] M. D. Cahn, R. W. Zobel, and D. R. Bouldin, "Relationship between root elongation rate and diameter and duration of growth of lateral roots of maize," *Plant Soil*, vol. 119, no. 2, pp. 271–279, Oct. 1989.
[40] Z. Chen, I. Newman, M. Zhou, N. Mendham, G. Zhang, and S. Shabala, "Screening plants for salt tolerance by measuring K^+ flux: A case study for barley," *Plant Cell Environ.*, vol. 28, no. 10, pp. 1230–1246, Oct. 2005.
[41] S. Shabala and T. A. Cuin, "Potassium transport and plant salt tolerance," *Physiol. Plantarum*, vol. 133, no. 4, pp. 651–669, Aug. 2008.

ZI-YANG WANG received the B.S. degree in electronic information science and technology from China Agricultural University, Beijing, China, in 2013, where he is currently pursuing the Ph.D. degree in agricultural electrification and automation. His current research interests include plant electrical signals and plant electrophysiological phenotypes.

JIN-HAI LI received the B.S. degree in mechanical design manufacture and automation from Linyi University, Linyi, China, in 2012, and the M.S. degree in mechanical manufacture and automation from Ningxia University, Yinchuan, China, in 2017. He is currently pursuing the Ph.D. degree in agricultural electrification and automation with China Agricultural University, Beijing, China.

QIAO ZHOU received the B.S. degree in textile engineering from the Inner Mongolia University of Technology, Hohhot, China, in 2014, and the M.S. degree in agricultural biological environment and energy engineering from Yunnan Agricultural University, Kunming, China, in 2017. He is currently pursuing the Ph.D. degree in computer science and technology with China Agricultural University, Beijing, China.

XIN-YU GAO received the B.S. degree in electronic and information engineering from China Agricultural University, Beijing, China, in 2016, where he is currently pursuing the M.S. degree in information and communication engineering.

LI-FENG FAN received the B.S. degree in electronic information science and technology and the M.S. degree in signal and information processing from China Agricultural University, Beijing, China, in 2013 and 2015, respectively, where he is currently pursuing the Ph.D. degree in agricultural electrification and automation.

YONG-QIAN WANG received the B.S. degree in electronic information science and technology from China Agricultural University, Beijing, China, in 2013, where he is currently pursuing the Ph.D. degree in agricultural electrification and automation. His current research interests include electrical impedance tomography applications in agriculture.

LIN XUE received the Ph.D. degree from China Agricultural University, Beijing, China, in 2016. She is currently a Lecturer with the Department of Smart City, Beijing Union University. Her current research interests include biosensors and their applications in agriculture.

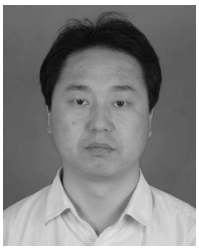

ZHONG-YI WANG received the Ph.D. degree from China Agricultural University, Beijing, China, in 2000. He is currently a Full Professor with the Department of Electronic Engineering, China Agricultural University. His current research interests include sensors in agriculture and precision instruments.

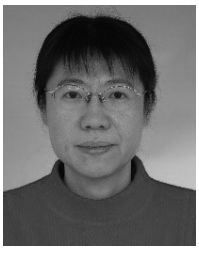

LAN HUANG received the Ph.D. degree from Tsinghua University, in 2004. Since 2011, she has been a Full Professor with China Agricultural University, Beijing, China. Her current research interests include bioelectronics and electronic applications in agriculture.